13th International Symposium on Particle Image Velocimetry – ISPIV 2019
Munich, Germany, July 22-24, 2019

Orthogonal dual plane time resolved PIV measurements in bypass transition

G. Balamurugan[1], Alakesh Chandra Mandal[1]*

[1] Department of Aerospace Engineering, Indian Institute of Technology Kanpur, UP - 208016, India.

* corresponding.alakeshm@iitk.ac.in

Abstract

An experimental investigation of the secondary instability characteristics in a flat plate boundary layer undergoing bypass boundary layer transition has been reported in this paper. Two types of streak instabilities, namely the sinuous and the varicose types are analyzed. Dual-plane time resolved particle image velocimetry (PIV) measurements at two different experimental configurations were conducted to shed light into the origin and nature of these streak secondary instabilities. The time-resolved stereoscopic PIV measurements in the wall normal spanwise (yz) plane at a streamwise location $x = 640$ mm reveals the nature of the streak secondary instability in that plane. A simultaneous two dimensional (2D) PIV data is acquired in the streamwise spanwise (xz) plane to associate the nature of instability with the stereo data. Sinuous instability occurs over a low speed streak which is lifted above the mean boundary layer edge whereas varicose instability occurs much closer to the wall well within the boundary layer. Secondly, using a simultaneous time resolved measurement in xy and xz, we have shown that a sinuous instability originates near the boundary layer edge. The varicose instability on the other hand occurs due to the interaction of a downstream low speed streak and an upstream high speed streak.

1 Introduction

Understanding, predicting and controlling laminar to turbulent transition has been a long lasting common agenda for most of the researchers in fluid mechanics and aerospace community. In spite of the enormous volume of research devoted on this over the years, there are still several aspects of transition that need further clarification mainly due to the highly sensitive nature of the transition route on the initial and boundary conditions. For example, depending on the level of inlet freestream turbulence (FST), boundary layer transition can be classified as natural and bypass transition. Natural transition occurs when the inlet FST is $< 0.1\%$ (e.g. Kachanov, 1994) and it is characterized by the formation of 2D Tollmein-Schlichting (TS) waves which then develop into three dimensional (3D) TS waves and finally break down to an intermittent turbulent spot. These spots spread while convecting downstream and merges to form a completely turbulent boundary layer. Bypass transition on the other hand occurs at moderate to high levels of FST (1%) and it completely bypasses the TS wave route of transition. It is dominated by the presence of high and low velocity streaks (e.g., Klebanoff, 1971; Matsubara and Alfredsson, 2001). These streaks grow in magnitude along the downstream direction and reaches a critical amplitude and they become susceptible to secondary instabilities. These secondary instabilities are of high frequency in nature compared to the low frequency streaks. In the past, these instabilities are classified as sinuous or varicose depending on whether the nature of oscillation is anti-symmetric or symmetric with respect to the underlying base streak when viewed along the streamwise spanwise (xz) plane (e.g., Brandt et al., 2004; Mans et al., 2005).

Generally, experimental streak instability studies in the literature were conducted on artificially generated steady streaks by placing either single or a row of roughness elements of varying heights inside the flat plate boundary layer (e.g., Asai et al., 2002; Fransson et al., 2005; Puckert and Rist, 2018). Although these streaks mimic the natural streaks to some extent, they still lack the unsteady streak interaction that is prominent in bypass transition. Further, the role of freestream turbulence in the excitation of streak secondary instability is absent. In the present study, natural bypass transition, characterized by unsteady high and low velocity streaks, is initiated over the flat plate by installing a parallel and a square mesh grid at the entrance of the wind tunnel test section. The freestream turbulent intensity level at the flat plate leading edge is around 2.5% of the freestream velocity for both the grids.

The origin of the instability in bypass transition has been a long standing concern where instability is either viewed to originate due to forcing from freestream on a lifted up shear layer or due to unsteady streak interactions close to the wall. Numerical results supporting both the viewpoint are available in the literature (Schlatter et al., 2008). Recently, based on the low speed (5Hz) simultaneous orthogonal dual plane PIV measurements, Balamurugan and Mandal (2017) speculated that an instability can originate near the edge of the boundary layer. To confirm that we have performed simultaneous time resolved PIV measurements in two orthogonal planes centered at $x = 700$ mm. It is found that, the sinuous type oscillation occurs in a shear layer lifted away from the wall and the varicose type oscillation is associated with a shear layer attached to the wall. Also, data supporting origin of oscillations close to the edge of the boundary layer were obtained. These results justify the need for a simultaneous time resolved measurements in clarifying existing confusions among the research community.

2 Experimental Setup

The present experiments were carried out in a suction type, open-circuit, low turbulence wind tunnel at the Department of Aerospace Engineering, IIT Kanpur, India. The dimensions of the tunnel test section are $3000\times61\times61$ cm^3. The streamwise turbulence level at the test section is found to be 0.1 % of the free-stream velocity, U_0. Boundary layer measurements were carried out on a transparent acrylic flat plate that was 12 mm thick, 1700 mm long and 610 mm wide. The flat plate has an asymmetric modified super elliptical leading edge with a thickness ratio of 7/24 between the working the non-working side of the plate. The present leading edge profile is suitable for experimental instability studies because it is aerodynamically optimized to produce minimum non-zero pressure gradient region and has a continuous first and second derivative at the juncture between the leading edge and flat portion thereby reducing the leading edge receptivity (Hanson et al., 2012). The downstream end of the plate is fixed with a trailing edge flap deployment of which can reduce the suction peak along the working side of the plate. Further details about the tunnel and the plate can be found in Balamurugan and Mandal (2017). Two different experimental configurations were utilized. The first configuration, as shown in figure 1, consists of a simultaneous stereoscopic and 2D planar time resolved PIV which are used to capture the instability events in the *yz* and *xz* planes respectively. The second configuration is used to view the instability in both *xy* and *xz* planes simultaneously. Here, we may mention that exact simultaneous data acquisition was not possible due to experimental and instrumental constraints. A few microsecond gap, approximately of the order of PIV δt between two consecutive images, are necessary for the safety of the equipment. However, this hardly change the flow and the interpretation of the results presented below. The schematic of the setup is shown in figure 1(a). In the following, x, y and z denote the streamwise, wall normal and spanwise directions, respectively, and u, v, w are their respective instantaneous velocity components.

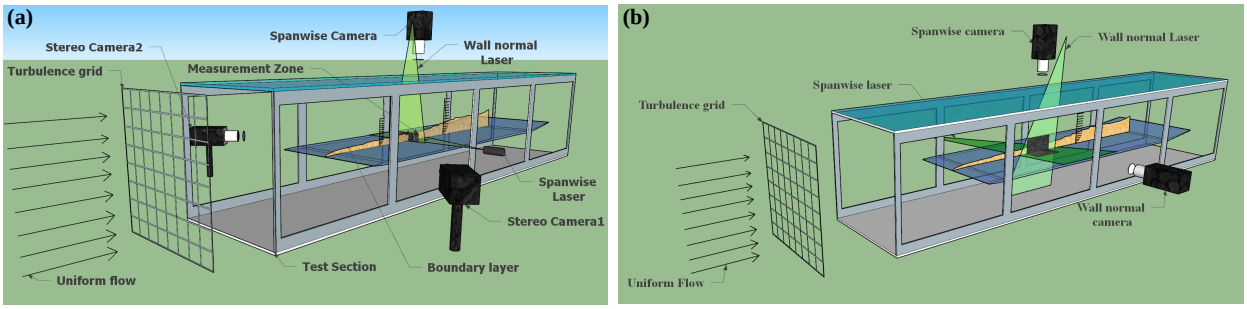

Figure 1: (a) Schematic of the experimental setup used for simultaneous stereoscopic and spanwise time resolved measurements. (b) Experimental setup for simultaneous time resolved PIV measurements in *xy* and *xz* planes.

The PIV setup consists of two dual head diode pumped Nd:YLF lasers (DM30 and DM40 model, Photonics Industries Inc, USA) emitting laser beam at a wavelength of 527 nm. The lasers can operate at a rate of 1 kHz in the dual pulse mode with a maximum energy of 30 mJ and 40 mJ per pulse, respectively. The beam from the laser head is channeled to the measurement region using an articulated light arm. A sheet forming optics at the end of articulated arm consists of a cylindrical lens which expands the laser beam into

a cylindrical sheet and a spherical lens for placing the waist of the light sheet at the required location. The flow is seeded with smoke particles of diameter $1\mu m$ using a fog generator (SAFEX, Dantec Dynamics). The smoke is distributed uniformly across the test section using a fan kept at the tunnel entrance. The smoke particles illuminated using the laser sheet are captured using high speed dual-exposure cameras. In configuration 1, the stereo images are acquired using two 4 Megapixel (MP) cameras (2336×1728 pixels, Y5, IDT, USA) and the spanwise 2D PIV images are captured using a 9 MP camera (3840×2400 pixels, O10, IDT, USA). The common region of interest for the stereo plane is 115×35 mm and it is centered with the centerline of the plate. The data were acquired at a frequency of 640 Hz in double exposure mode. To reduce the reflection of the stereo plane laser from the plate on the spanwise camera, it is shifted downstream by a distance of around 7 mm. The viewing angle between the two stereo cameras were maintained at 90^o since the streamwise velocity has the maximum magnitude in a boundary layer. For the second configuration, both the *xy* and *xz* plane data were acquired using two IDT Y5 cameras at 640 Hz. The stereo cameras were fitted with two 85 mm tilt shift lenses (PC-E MICRO NIKKOR 85 mm F/2.8D) which were adjusted accordingly so that Scheimpflug condition was met for both the cameras. The 2D PIV cameras were equipped with 100 mm macro planar lens (Carl Zeiss, f/2 Makro-Planar). The stereo and the 2D PIV images were processed using commercial PIV software, provision-XS, IDT.

3 Results and Discussions

The instabilities that develop during a laminar turbulent transition induced by freestream turbulence are random, highly unsteady and three dimensional in nature. These instabilities can grow both spatially and temporally. Hence, with conventional low repetition rate 2D PIV technique, it is difficult to characterize such instability events. This justifies the need for simultaneous, orthogonal, time-resolved, high speed, stereo PIV data.

3.1 Stereo-PIV results

Stereoscopic PIV is done to visualize the streak configuration in the *yz* plane during the secondary instability. The top row in Figure 2(a) shows the time evolution of the nature of streak oscillation in the *yz* plane when a sinuous instability is occurring in the *xz* plane. A white dashed line shows the mean location of the boundary layer thickness. The instability always develops over a low speed streak compared to the high speed streak. It is observed that the streak undergoing sinuous instability is lifted much higher than the mean boundary layer edge. The varicose instability is characterized by symmetric oscillation with respect

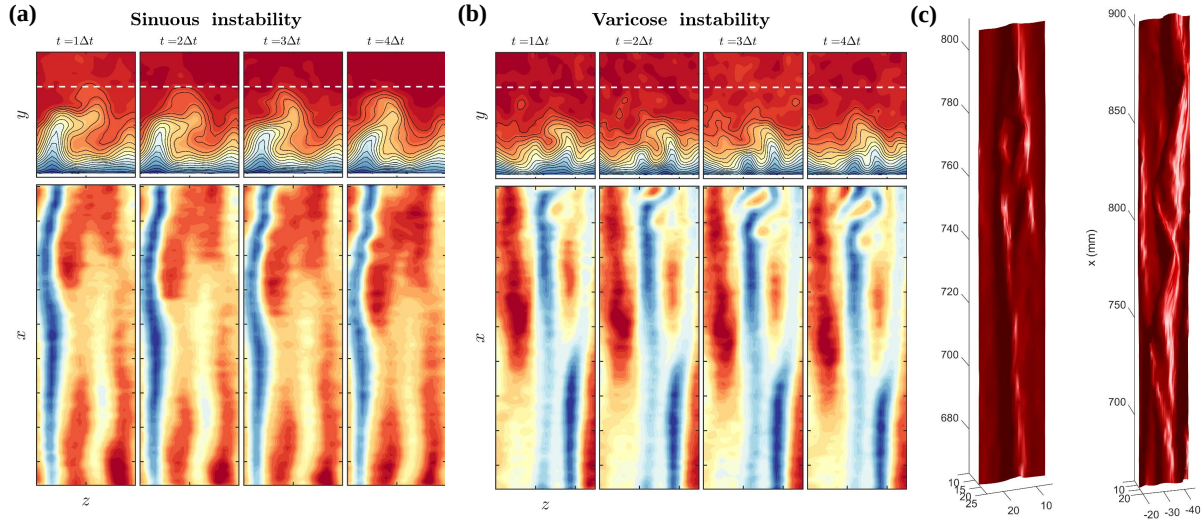

Figure 2: Time evolution of (a) sinuous and (b) varicose instability in simultaneous *yz* and *xz* planes.(c) Iso contour of a streamwise velocity showing the three dimension reconstruction of the varicose and sinuous instability from the time resolved stereoscopic data.

to the base streak. The time evolution of the varicose instability acquired in *yz* and *xz* planes simultaneously are given in figure 2(b). One can observe that it occurs close to the wall compared to the sinuous case. Since we have a time resolved PIV data in the *yz* plane, we can reconstruct the three dimensional form of the instability if one assumes Taylor's hypothesis. Although the instabilities are convective in nature, it does not capture the exact scenario. However, such an attempt is made just to have a three dimensional picture of the instability which has not experimentally done earlier. Figure 2(c) shows the isocontour of low speed streaks undergoing instability identified using streamwise velocity values of U=2.5 and 4 m/s for the varicose and sinuous instability respectively. One can clearly identify the symmetric and asymmetric nature of oscillation from these plots.

It was numerically found that that varicose instability occurs due to dominant influence of wall normal shear whereas sinuous instability is dominated by spanwise shear (e.g. Brandt et al., 2004; Hack and Zaki, 2014). Because of the random nature of the occurrence of these instability events, researchers have used artificial steady streaks (i.e. streaks generated using roughness elements, wall suction, screens) to clarify the role of flow shear (Philip et al., 2016). However, such a clarification is absent for natural streaks generated in bypass transition. Since the present stereo measurements allow such an analysis, we present the instantaneous shear profiles for a sinuous and varicose instability in figure 3. The top row shows the contour plot of instantaneous streamwise velocity normalized with the mean freestream velocity, U_0. In second row, we have the flooded contour plots of wall normal shear in figure 3(Ic) and the spanwise shear is shown in figure 3(Id). Further, the contour lines of streamwise velocities are plotted to show the region where the peak shear values are observed. The third row figures (e) and (f) show the distribution of streamwise velocity and its first derivative along the dashed in figures (c) and (d), respectively. The wall normal shear is plotted with respect to y and the spanwise shear is plotted with respect to z. One can find that the wall normal and the spanwise shear are of comparable magnitude (1.5 and 1) for a sinuous instability whereas the numerical values of these shears (3.6 and 1) for varicose instability are not comparable. But one cannot see a clear dominance of spanwise shear for the sinuous instability. Hence one has to compare the instability events generated by steady and natural streaks, which is done as a part of our future work.

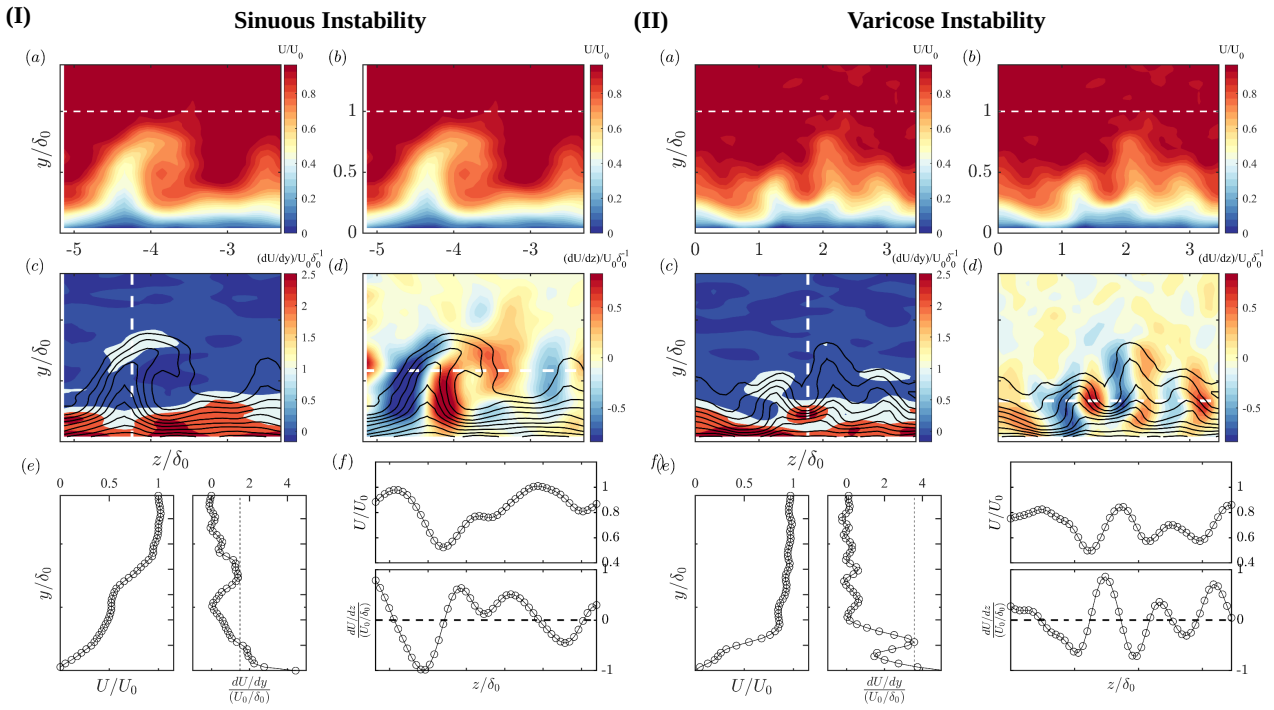

Figure 3: Comparison of wall normal and spanwise shear for (I) sinuous and (II) varicose instabilities. (a-b) Streamwise velocity contour of sinuous and varicose oscillation. Contour lines of streamwise velocity over the floods of (c) wall normal and (d) spanwise shear. (e) Wall normal profiles of wall normal shear. (f) spanwise profiles of spanwise shear. The dashed line in first row indicates the mean boundary layer thickness. The white dashed line in second row indicates the location where the shear profiles are extracted. The dashed line in the third row indicates the peak value of wall normal shear.

3.2 Simultaneous TR-PIV results

Figure 4 shows the time evolution of sinuous and varicose instabilities in two (*xy* and *xz*) orthogonal planes. The left side column in figure 4(a) shows the spanwise vorticity contours in the *xy* plane. The presence of inclined shear layer can be identified due to the lift up of the low speed streak and as time progresses one can observe a wave like secondary instability developing near the boundary layer edge. This instability convects with the flow, grows in amplitude and eventually reaches the wall. The simultaneous spanwise (*xz* plane) view measured at dashed line location in the *xy* plane is shown along the right side column of figure 4(a). Contours of streamwise velocity show the presence of high (red contours) and low (blue contours) speed streaks. Also shown using dashed white line in the figure is the location of wall normal plane where data for the *xy* plane is measured. Starting from the third time instant we can find the development of antisymmetric sinuous oscillation in the low speed streak. This oscillation grows and convects downstream with the flow thus ensuring the convective nature of streak secondary instability. One important thing to note is that oscillations are evident in the *xz* plane only from the third time instant whereas in the *xy* plane it is much clear right from the first time instant. This shows that sinuous instability develops close to the boundary layer edge and then eventually propagates into the boundary layer. This opens the question on the role of freestream perturbations in the triggering of such instabilities. We do not have much information to comment of such a role which can be thought of as a future work.

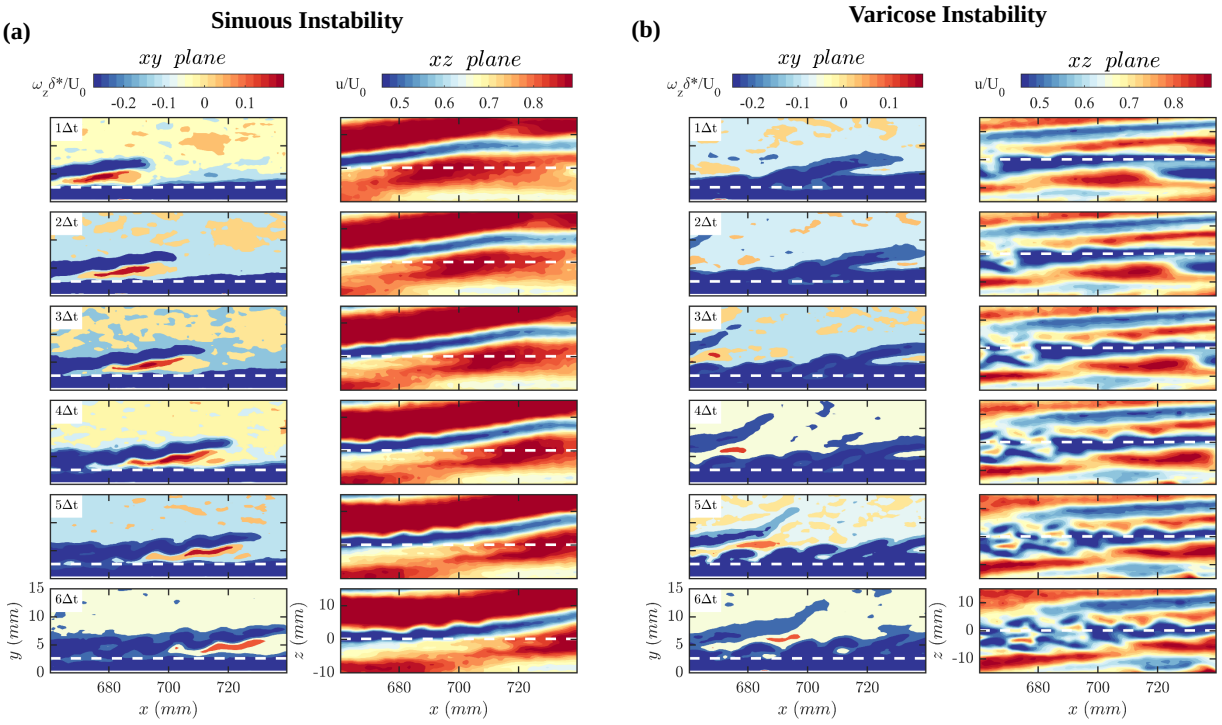

Figure 4: Time evolution of (a) Sinuous and (b) Varicose instability in simultaneous *xy* and *xz* planes.

Similarly, the time evolution of the varicose instability is shown in figure 4(b). The left column shows the wall normal view using the contours of spanwise vorticity and the right column shows the corresponding spanwise view using streamwise velocity contours. In contrast to the sinuous instability the shear layers are much closer to the wall for the varicose instability. This is consistent with the stereo PIV results reported earlier and confirms the speculation made by Balamurugan and Mandal (2017) using low speed (5 Hz) PIV measurements.

4 Conclusion

The spanwise wall normal *yz* view of a natural streak undergoing secondary instability is presented for the first time using time resolved stereoscopic PIV measurements. With a simultaneous 2D PIV in the

xz plane, we could relate and confirm that low speed streak gets lifted up even above the mean boundary layer thickness during sinuous streak instability. Whereas it occurs much closer to wall for a varicose instability. Further, the stereo PIV data enabled us to relate the spanwise and wall normal shear for a natural streak undergoing bypass transition. The shears are of the same order for the sinuous instability whereas the wall normal shear dominates the varicose instability. Moreover using simultaneous time resolved PIV measurements in *xy* and *xz* planes, we could confirm that a sinuous instability can develop close to the boundary layer edge thereby confirming the speculations made in Balamurugan and Mandal (2017).

Acknowledgements

The authors would like to thank Professors K. Poddar, D. Das, A. Kushari, S. Mittal, S. Kumar and V. Shankar for their support in our experimental campaign. Financial support from AR and DB through a project (1880) is also gratefully acknowledged. We are grateful to Mr. K. Selvaraj, Sc F, ADE, DRDO, Bangalore, for fruitful discussions. We also thank Mr Y. Arafath, Dr K. K. Bharadwaj, Dr C. L. Dora and Mr M. Aniffa for their experimental help and fruitful discussions.

References

Asai M, Minagawa M, and Nishioka M (2002) The instability and breakdown of a near-wall low-speed streak. *J Fluid Mech* 455:289–314

Balamurugan G and Mandal A (2017) Experiments on localized secondary instability in bypass boundary layer transition. *J Fluid Mech* 817:217–263

Brandt L, Schlatter P, and Henningson DS (2004) Transition in boundary layers subject to free-stream turbulence. *J Fluid Mech* 517:167–198

Fransson JH, Brandt L, Talamelli A, and Cossu C (2005) Experimental study of the stabilization of tollmien–schlichting waves by finite amplitude streaks. *Physics of Fluids* 17:054110

Hack M and Zaki T (2014) Streak instabilities in boundary layers beneath free-stream turbulence. *Journal of Fluid Mechanics* 741:280–315

Hanson RE, Buckley HP, and Lavoie P (2012) Aerodynamic optimization of the flat-plate leading edge for experimental studies of laminar and transitional boundary layers. *Experiments in fluids* 53:863–871

Kachanov YS (1994) Physical mechanism of laminar-boundary-layer transition. *Ann Rev Fluid Mech* 26:411–482

Klebanoff PS (1971) Effect of freestream turbulence on the laminar boundary layer. *Bull Amer Phys Soc* 10:1323

Mandal AC, Venkatakrishnan L, and Dey J (2010) A study on boundary layer transition induced by freestream turbulence. *J Fluid Mech* 660:114–146

Mans J, Kadijk EC, de Lange HC, and van Steenhoven AA (2005) Breakdown in a boundary layer exposed to free-stream turbulence. *Exp Fluids* 39:1071–1083

Matsubara M and Alfredsson PH (2001) Disturbance growth in boundary layers subjected to free-stream turbulence. *J Fluid Mech* 430:149–169

Philip J, Karp M, and Cohen J (2016) Streak instability and generation of hairpin-vortices by a slotted jet in channel crossflow: Experiments and linear stability analysis. *Physics of Fluids* 28:014103

Puckert DK and Rist U (2018) Experiments on critical reynolds number and global instability in roughness-induced laminar–turbulent transition. *Journal of Fluid Mechanics* 844:878–904

Schlatter P, Brandt L, de Lange HC, and Henningson DS (2008) On streak breakdown in bypass transition. *Phys Fluids* 20:101505–1–101505–15